Taylor & Francis
Taylor & Francis Group

Journal of Toxicology and Environmental Health, Part A
Current Issues

ISSN: 1528-7394 (Print) 1087-2620 (Online) Journal homepage: www.tandfonline.com/journals/uteh20

Pulmonary inflammatory and fibrogenic responses in rats following intratracheal instillation of dusts from natural and engineered stones

W. Kyle Mandler, Chaolong Qi, Drew Thompson, Torrie A. Crabbs, Ann F. Hubbs, Alycia K. Knepp, Sarah Keeley, Samantha Service, Lori A. Battelli, Sherri A. Friend, James M. Antonini, Bailey D. Riggleman & Yong Qian

To cite this article: W. Kyle Mandler, Chaolong Qi, Drew Thompson, Torrie A. Crabbs, Ann F. Hubbs, Alycia K. Knepp, Sarah Keeley, Samantha Service, Lori A. Battelli, Sherri A. Friend, James M. Antonini, Bailey D. Riggleman & Yong Qian (2026) Pulmonary inflammatory and fibrogenic responses in rats following intratracheal instillation of dusts from natural and engineered stones, Journal of Toxicology and Environmental Health, Part A, 89:8, 363-382, DOI: 10.1080/15287394.2025.2571405

To link to this article: https://doi.org/10.1080/15287394.2025.2571405

JOURNAL OF TOXICOLOGY AND ENVIRONMENTAL HEALTH, PART A
2026, VOL. 89, NO. 8, 363–382
https://doi.org/10.1080/15287394.2025.2571405

Taylor & Francis
Taylor & Francis Group

Pulmonary inflammatory and fibrogenic responses in rats following intratracheal instillation of dusts from natural and engineered stones

W. Kyle Mandler[a], Chaolong Qi[a], Drew Thompson[a], Torrie A. Crabbs[b], Ann F. Hubbs[a], Alycia K. Knepp[a], Sarah Keeley[a], Samantha Service[a], Lori A. Battelli[a], Sherri A. Friend[a], James M. Antonini[a], Bailey D. Riggleman[a], and Yong Qian[a]

[a]Health Effects Laboratory Division, National Institute for Occupational Safety and Health, Morgantown, WV, USA; [b]Experimental Pathology Laboratories, Inc, Durham, NC, USA

ABSTRACT

Engineered stone (ES) fabrication workers face risks from exposure to respirable crystalline silica (RCS), leading to accelerated silicosis. Toxicological data to elucidate pulmonary effects attributed to ES dusts, particularly those with varying compositions, are lacking. This study aimed to determine pulmonary effects following intratracheal instillation (IT) of ES dust in rats. Male Sprague-Dawley rats received a single 10 mg IT dose of dust from one of three ES types containing varying amounts of crystalline silica (CS) (ES A [high CS], ES B [mid CS], ES C [low CS]), or granite, MIN-U-SIL 5 (MS 5, positive control), or saline. Pulmonary inflammation and fibrosis were assessed via bronchoalveolar lavage fluid (BALF) analysis and lung histology at 1-, 21-, and 84-days post-exposure. Early BALF inflammation as evidenced by increased levels of neutrophils and lymphocytes, and cytotoxicity by elevated LDH activity was found in all exposure groups. Neutrophils primarily correlated with higher CS content (MS 5, ES A, ES B). Persistent inflammation comparable with pure silica was noted by increased levels of neutrophils and macrophages and cytotoxicity by elevated LDH activity at 21- and 84-days post-exposure was most pronounced in MS 5 and high-CS ES A groups. By 84-day post-exposure, granulomatous inflammation in lung, BALF and lymph node, was associated with alveolar lipoproteinosis, type II epithelial changes, lymph node and alveolar fibrosis. Toxicity appeared to be driven by complex interactions between silica and trace metal content of dust. These findings warrant further research to assess combined effects of particle characteristics and chemical co-exposures.

Introduction

Engineered stone (ES) composites occupy a prominent niche within the global construction industry, offering a compelling alternative to natural stones in various applications. These materials are manufactured by combining a high proportion as much as 95% by weight of crystalline silica (Ramkissoon et al. 2024) contained in crushed stone aggregates, with a polymer resin binder constituting the remaining weight to form a solid surface (Phillips, Johnson, and Johnson 2013). In comparison, natural stones such as granite usually contain lower silica content (10–45%) (OSHA 2015). The most common resin type is polyester epoxy, such as diglycidyl ether derived from bisphenol A (Carvalho et al. 2018). Pigments, often metal oxides (Bustillo Revuelta 2021), may also be incorporated into the ES matrix to achieve a desired aesthetic and broader color palette. The inclusion of silica imbues ES with exceptional mechanical properties as evidenced by conversion to a higher degree of strength and hardness, rendering the material resistant to scratches, cracks, and heat (Santos, Crovace, and Zanotto 2019). The incorporation of polymers further bolsters these beneficial attributes, contributing to a non-porous composition that effectively resists staining (Caesarstone 2021). By virtue of these physical qualities, ES has become a highly sought-after material for countertops and flooring applications.

The demand for countertops is projected to surge at a compound annual growth rate of 6.5%

CONTACT W. Kyle Mandler wmandler@cdc.gov Pathology and Physiology Branch, Health Effects Laboratory Division, National Institute for Occupational Safety and Health, 1095 Willowdale Road, Morgantown, WV 26505, USA

This article has been republished with minor changes. These changes do not impact the academic content of the article.
Supplemental data for this article can be accessed online at https://doi.org/10.1080/15287394.2025.2571405

between 2023 and 2030, fueling industry expansion and a significant rise in the manufacturing workforce, which is concentrated in small fabrication shops (Grand View Research 2023). This growth presents a significant occupational health risk, as fabrication processes such as cutting and grinding generate airborne dust containing respirable crystalline silica (RCS). This concern is particularly critical, as studies documented worker exposures exceeding the Occupational Safety and Health Administration (OSHA) Permissible Exposure Limit (PEL) of 50 $\mu g/m^3$ (Qi and Echt 2016; Qi and Lo 2016; Zwack, Brueck, and Qi 2016). The risk is often exacerbated in small businesses that may lack resources to implement effective training and exposure control measures. Fabrication processes, such as cutting, grinding, and polishing, conducted in both workshop and installation environments generate airborne dust containing RCS and other composite materials. This poses a significant occupational health risk to the expanding workforce in this sector, specifically through exposure to RCS. Such exposure is a recognized cause of progressive, irreversible pulmonary silicosis, which might lead to disability or mortality, and was linked to an elevated incidence of autoimmune and immune system disorders (Anlar et al. 2017; Pollard 2016), pulmonary tuberculosis (Rose et al. 2019), lung carcinoma (Sato, Shimosato, and Klinman 2018), obstructive pulmonary disease (Hnizdo and Vallyathan 2003), pulmonary toxicity (Umbright et al. 2017) and renal disease (Millerick-May et al. 2015). Alarming outbreaks of silicosis in the stone countertop industry were reported across the USA and internationally (Rose et al. 2019). Recognizing this threat, OSHA and NIOSH jointly issued a 2015 Hazard Alert document emphasizing the dangers of airborne RCS in the stone countertop industry (OSHA 2015).

In addition to particle emissions, cutting ES releases volatile organic compounds (VOC) (Ramkissoon, Gaskin, Hall, et al. 2022). Analysis of organic compounds emitted during dry-cutting of ES identified elevated levels of respiratory irritants. Phthalic anhydride, the most abundant organic component (26–85%), carries a respiratory sensitization notation. In addition, styrene, the primary VOC emitted during cutting, occurs jointly with other irritants including benzene and toluene. These findings demonstrate that workers fabricating ES face concurrent exposure to hazardous RCS dust and organic irritants. It remains to be determined if there are synergistic adverse pulmonary effects resulting from this mixed exposure.

A notable characteristic of ES-associated silicosis is its relatively short latency period, often termed "accelerated" silicosis, distinguishing it from traditional cases linked to other high-risk occupations, such as mining and sandblasting. Stone countertop workers tend to develop the disease at a younger age and with considerably less exposure time than individuals in traditional high-risk professions. The specific factors within ES exposure that contribute to this accelerated progression remain an area of active investigation. Further, investigators indicated that disease progression, with simple silicosis transforming into progressive massive fibrosis (PMF) occurred even years after exposure cessation (Ramkissoon, Gaskin, Thredgold, et al. 2022).

Despite conclusive evidence for silicosis development following RCS exposure; crucial knowledge gaps remain. The mechanisms underlying ES silicosis short latency periods and specific hazards associated with RCS emissions, especially in the presence of polymeric resins and other components found in ES products (Ramkissoon, Gaskin, Hall, et al. 2022), are not well-understood. Both cristobalite and quartz contribute to the CS composition of ES emissions (Ramkissoon et al. 2024). There have been a few notable efforts to characterize ES dust toxicity *in vitro*. Pavan et al. (2016) observed that while morphologically similar to quartz particles, ES particles contained higher amounts of trace metals and were not as cytotoxic to exposed alveolar macrophage mouse lung (MH-S) or human bronchial lung epithelial (BEAS-2B) cells. Both quartz (the major type of CS) and all ES dusts tested induced epithelial–mesenchymal transition (EMT) (Pavan et al. 2016), which may explain the mechanisms involved in the widespread development of fibrosis among occupationally exposed workers. Ramkissoon et al. (2024) examined the relative cytotoxicity of 50 different types of ES using principal component analysis (PCA) to

determine the contributions of trace metals. Ramkissoon et al. (2024) noted that both cobalt (Co) and aluminum (Al) were significantly associated with macrophage toxicity.

To date, there have been no apparent *in vivo* studies investigating ES dust-induced toxicity. This study aimed to determine the pulmonary effects following intratracheal instillation (IT) of ES dust in rats, utilizing materials with varying RCS content in conjunction with natural granite and pure silica as controls. These findings might inform future research endeavors seeking to unravel the toxicological mechanisms underlying these complex materials.

Methods

Dust generation system and characterization

Dust generation and collection using a controlled lab system designed and operated for characterizing the generation rate of respirable dust during grinding is described in Thompson and Qi (2022). Bulk dust samples were collected post-experiment for use in the present study, followed by thorough chamber cleaning to prevent contamination between stone types. The morphology and size distribution of ES dust particles were characterized using field-emission scanning electron microscopy (FE-SEM). A 0.1% (w/w) suspension of particles in saline was prepared and subjected to sonication for 3 min (energy input = 1000 J). This suspension was diluted to a final concentration of 0.02% (w/w), and 0.5 ml was filtered through a 0.2 µm pore-size polycarbonate filter (Sterlitech Corp., Kent, WA). A representative section from each filter was imaged at 2000x magnification using a 20 kV accelerating voltage (Hitachi S-4800, Hitachi High-Technologies America, Inc., Dallas, TX). Ten fields of view were randomly selected, and particle diameters were manually measured using ImageJ software (National Institutes of Health, Bethesda, MD).

Metals characterization

The samples were digested and analyzed for elements according to NIOSH Method 7303 modified for bulk matrix (NMAM 4th Edition). Approximately 0.1 g of each bulk sample was placed in a clean 50-ml polypropylene centrifuge tube. Five ml nitric acid (Fisher lot 240,238) and 5 ml hydrochloric acid (J.T. Baker lot 24D1562005) were added to each tube. The tubes were placed on a hot block and heated to a temperature of 95°C for 30 min. The samples were removed from the hot block, allowed to cool, and diluted to a final volume of 50 ml with deionized water. All Limit of Detection (LOD), Quality Control (QC), and client samples were digested in the same manner. The samples were analyzed using an Agilent 5800 Inductively Coupled Plasma – Optical Emission Spectrometer ICP-OES (Santa Clara, CA) with the conditions described in Table 1.

TABLE 1. ICP-OES Settings

Parameter	Value	Unit
RF Power	1400	watts
Plasma Flow (Argon)	13	L/min
Auxiliary Flow (Argon)	1	L/min
Nebulizer Flow (Argon)	0.65	L/min
Sample Pump Speed	12	rpm
Replicate Count	3	

Animals

Male Sprague-Dawley (SD) rats (6–7 weeks old, weighing 200–225 g) were purchased from Hilltop Lab Animals (Scottdale, PA) and housed in a specific pathogen-free, AAALAC-accredited facility in ventilated polycarbonate cages, 4 rats per cage. Rats were acclimated for at least 7 days prior to start of the study. The facility provided a controlled environment with HEPA-filtered air, a temperature of 22 ± 2°C, and a humidity of 40–60%. Animals were fed irradiated Teklad 2918 diet (Madison WI) and provided with ALPHA-dri®/Teklad sani-chips bedding mix and tap water *ad libitum*. The study protocol was reviewed and approved by the CDC-Morgantown Institutional Animal Care and Use Committee, which is accredited by AAALAC International.

Experimental design

Rats were assigned to exposure groups ($n = 8$ per group, per post-exposure time point, 144 total) using a randomized complete block design were exposed to either suspensions containing dust from grinding granite, engineered stone A, B or C (ES A, ES B, ES C), MIN-U-SIL (MS 5), or saline control using intratracheal (IT) instillation

following the previously published protocol (Blackford et al. 1997). The day of each exposure, each dust sample was suspended at 20 mg/ml in sterile saline and ultrasonicated on ice for 30 s at 40% amplitude using a Branson 450 ultrasonicator (Emerson Industrial Automation, St. Louis, MO). The suspensions were brought to room temperature and vortexed for an additional 30 sec immediately prior to exposure. Rats were anesthetized with intraperitoneal (IP) injection of sodium methohexital. Once fully anesthetized, rats were placed on a slant board using a rubber band by the incisor teeth. Rats were IT instilled with 0.5 ml sterile saline control or dust suspended in 0.5 ml saline (10 mg dust/rat) via a 20-gauge feeding needle. Once the rat was exposed, it was removed from the slant board and placed on its left side to fully recover. Animals were monitored immediately, 1 and 8 h after exposure for full recovery. The rats were given wellness checks and weights taken weekly to monitor health of animals. Following exposure, each rat was assigned to either 1, 21, or 84-day post-exposure groups. All exposed animals survived the duration of the post-exposure period. At the conclusion of the post-exposure period, each animal was euthanized via pentobarbital overdose and bodyweight recorded.

BALF analysis

BALF collection and cytology

Three ml cold PBS was passed into the right lung via a tracheal cannula; the lung was massaged for 30 sec, cold PBS was withdrawn, and the process repeated a second time, yielding the first fraction of BALF. A second BALF fraction was collected by repeating the aforementioned process using 3 ml aliquots of PBS until a 9 ml volume was recovered. The two BALF fractions were centrifuged (800xg, 10 min, 4°C), and supernatant from fraction one and the combined cell pellets from both fractions were kept for further analysis (supernatant from fraction two was discarded). The supernatant was used to measure lactate dehydrogenase (LDH) activity and cytokine levels. The pellet was resuspended in 1 ml PBS (Gibco, Waltham, MA)), and used for a total cell count and cell differential (Beckman Coulter Multisizer 4 particle counter, Coulter Electronics, Hialeah, FL) as previously described (Farcas et al. 2020).

BALF LDH activity

LDH activity was determined in the first acellular fraction of BALF. Analyses were conducted on the Synergy H1 Microplate Reader (Agilent Technologies, Lexington, MA) utilizing the Pierce™ Lactate Dehydrogenase Reagent Set (Pointe Scientific; Lincoln Park, MI).

BALF cytokines/chemokines

A V-PLEX Pro-inflammatory Panel 2 Rat Kit (MSD, Rockville, MD) was utilized to quantify cytokine levels in BALF samples. Data acquisition was performed using a QuickPlex SQ 120 plate reader (MSD, Rockville, MD). This assay enabled measurement of the following analytes: IFN-γ, IL-1β, IL-4, IL-5, IL-6, IL-10, IL-13, KC/GRO, and TNF-α.

Blood cell counts and chemistry analysis

Blood collected in EDTA-containing and clot-activator-/polymer gel-containing vacutainers were processed and analyzed as previously described in Farcas et al. (2020).

Characterization of blood cells and hematological parameters

A complete blood count (CBC) was performed for each sample 30–45 min after collection using a ProCyte Dx Hematology Analyzer (IDEXX Laboratories, Inc., Westbrook, ME).

Lung and nasal passages histopathology evaluation

The unlavaged left lung was inflated and fixed with 10% neutral buffered formalin (NBF), embedded in paraffin, cut at 5 µm on Schott slides, and stained with hematoxylin and eosin (H&E) or picrosirius red for histopathological evaluation. The stained slides of lung (H&E and picrosirius red) and tracheobronchial lymph node (H&E) were submitted to Experimental Pathology Laboratories (EPL®), Inc., Durham, NC for review by a board-certified

veterinary pathologist.. The pathologist examined all slides by brightfield microscopy and used a polarizer to evaluate the tissue for the presence of polarized material. Lung findings were graded for severity (0 = none, 1 = minimal; 2 = mild; 3 = moderate; 4 = marked; and 5 = severe) and distribution (0 = none, 1 = focal; 2 = locally extensive; 3 = multifocal; 4 = multifocal to coalescing; and 5 = diffuse). A pathology score was calculated for each finding with the score equaling the sum of the severity and distribution scores. Lymphoid findings, to include findings in the bronchus-associated lymphoid tissue (BALT) in the lung, were only assigned a severity grade.

Statistics and linear regression analysis

Statistical analyses were performed using SAS/STAT v9.4 (Windows), with significance set at $p < 0.05$. Two-way ANOVA (treatment × duration) was used to analyze measured variables, followed by Fisher's LSD post hoc tests for relevant group comparisons.

Simple linear regression was employed to examine the association between % silica content with selected BALF and blood endpoints. To further understand the role that the trace metals and silica played on the variation in endpoint results, PCA, Pearson correlations between silica, the trace elements and measure endpoints, and stepwise regression analysis was performed. PCA and Pearson correlations displayed high multicollinearity between several metals resulting in more complex multiple linear regression models to exhibit less reliable statistical inference. However, the models that were created often displayed several trace metals as significant predictors. In regard to predictive inference, models that accounted for the variation in time along with the stone composition resulted in a 30% rise in variation explained by the endpoint. A significance level of 5% was used for all statistical analysis.

Results

Dust characteristics

Figure 1A depicts a representative EM micrograph (of ES A) used to generate data depicted in 1B-D. MS 5 exhibits the smallest particle sizes across all metrics, including minimum (0.1980 μm), maximum (8.148 μm), mean (0.9033 μm), and geometric mean (0.6765 μm). Granite dust showed intermediate particle sizes, with a mean of 1.347 μm and a relatively narrow geometric standard deviation factor (1.857), suggesting lower size variability. The ES A samples generally contained larger particle sizes than both MS 5 and granite. ES A possessed the largest maximum size (12.61 μm) and range (12.47 μm). ES B showed the largest mean (1.630 μm) and geometric mean (1.141 μm) among ES samples. ES C contained the smallest maximum and range, within the ES samples. The smaller particle size of MS 5 may contribute to the observed enhanced toxicity on a mass basis compared to the other tested materials, likely due to factors such as higher surface area-to-volume ratio and increased penetration into biological systems.

The contents of CS among the test stones were determined previously. As reported by Thompson and Qi (2022), ES A and granite presented a higher % of crystalline silica (60% and 30% respectively), while ES B a lower 23%, and ES C with CS below the LOD.

In this study, the contents of metals were determined. The results of our metals analysis (Table 2) indicated that ES C possessed significantly higher % aluminum (Al) and calcium (Ca) compared to ES A, ES B, and granite. Cobalt (Co), copper (Cu), iron (Fe), lithium (Li), magnesium (Mg), manganese (Mn), nickel (Ni), phosphorus (P), potassium (K), strontium (Sr), tin (Sn), and titanium (Ti) were present in varying trace amounts across the samples, with some elements being below the LOD or limit of quantification (LOQ) in certain samples.

BALF

Cytology

To determine pulmonary injury, the total cells as well as the differentiated cell counts in bronchoalveolar lavage fluid (BALF) were measured (Figure 2). At day 1 post-exposure, lymphocyte counts were elevated across all exposure groups relative to saline control, indicating a rapid, generalized immune response to instilled dusts. Concurrently, polymorphonuclear neutrophils

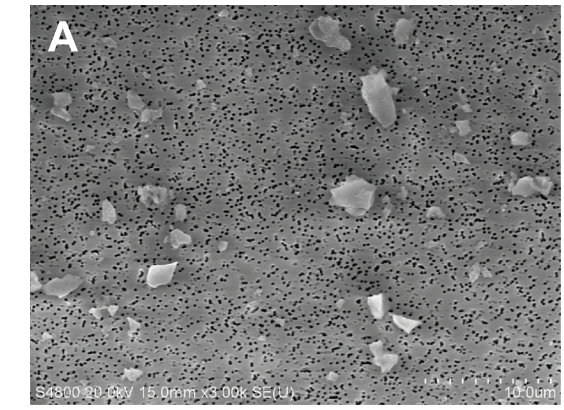

B

	Min U Sil 5	Granite	ES A	ES B	ES C
Number of values	219	800	474	376	297
Minimum	0.20	0.23	0.13	0.21	0.20
Maximum	8.15	9.61	12.61	10.86	7.39
Range	7.95	9.38	12.47	10.65	7.19
Mean	0.90	1.35	1.46	1.63	1.27
Std. Deviation	0.89	1.08	1.45	1.71	1.09
Std. Error of Mean	0.06	0.04	0.07	0.09	0.06
Geometric mean	0.68	1.09	1.09	1.14	0.99
Geometric SD factor	2.05	1.86	2.06	2.23	1.98

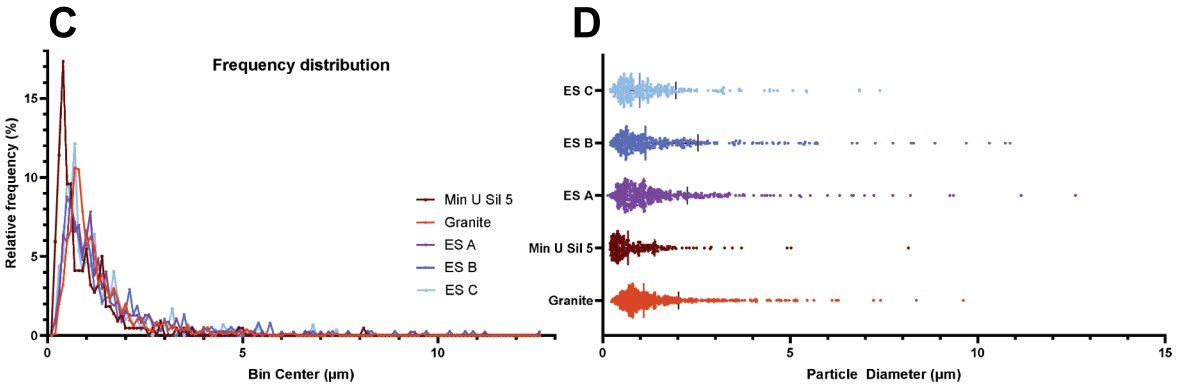

FIGURE 1. Characterization of ES particle size distribution. (A) scanning electron micrograph (SEM) of ES a particles deposited on a filter membrane (~0.2 µm black circles are filter pores). Scale bar = 10 µm. (B) tabulated ImageJ data representing the particle size distribution parameters all reported in micrometers (µm). (C) frequency distribution histograms illustrating the size distribution for each particle type X-axis: Bin Center (µm); Y-axis: relative frequency (%). (D) stacked individual particle size measurements for each particle type displayed as beeswarm plots. X-axis: particle diameter (µm).

(PMNs) were significantly elevated in MS 5, ES A, and ES B groups, indicative of an acute inflammatory reaction to these specific materials. Macrophage levels remained unchanged at this initial time point except for in the MS 5 group, consistent with their typically slower response time.

By day 21 post-exposure, a more differentiated response was detected. Lymphocyte elevation persisted only in the MS 5, ES A, and ES C groups, indicating a persistent lymphocytic presence in the lungs in response to these materials. ES B Lymphocytes appeared to remain increased at this timepoint, but were not markedly different from control due to enhanced variability. Macrophage counts were significantly higher in the MS 5 and ES A groups, reflecting the ongoing phagocytic clearance of these materials. PMNs rise remained restricted to MS 5 and ES A groups, indicative of persistent acute inflammation or a delayed resolution (Figure 2).

At day 84 post-exposure, a resurgence of inflammation was evident. Lymphocyte counts were again increased across all exposure groups relative to saline controls. This widespread lymphocyte elevation suggests establishment of a chronic inflammatory process or a delayed-type hypersensitivity reaction. Macrophage levels remained higher in MS 5 and ES A groups, consistent with their continued role in clearing these persistent irritants. Critically, PMNs counts were significantly elevated across all exposure groups at day 84. This widespread PMNs influx indicated a renewed wave of acute inflammation, suggesting ongoing lung damage or development of a chronic inflammatory state (Figure 2).

These data collectively demonstrate that MS 5 and ES A consistently elicited the most pronounced and persistent inflammatory responses across all cell types and time points. The reemergence of elevated lymphocytes and, particularly, PMNs at day 84 post-exposure across all groups indicates

TABLE 2. Dust Sample Crystalline Silica and Trace Metal Percentage

Element	ES A	ES B	ES C	Granite
Crystalline Silica (SiO2) (Thompson et al. 2023)	60%	23%	< LOD	30%
Aluminum (Al)	0.03%	0.08%	1.20%	0.42%
Antimony (Sb)	<LOD	<LOD	<LOD	<LOD
Arsenic (As)	<LOD	<LOD	<LOD	<LOD
Barium (Ba)	0.00%	0.00%	0.00%	0.00%
Beryllium (Be)	<LOQ	<LOQ	<LOQ	0.00%
Cadmium (Cd)	<LOD	<LOD	<LOD	0.00%
Calcium (Ca)	0.01%	0.09%	11.00%	0.15%
Chromium (Cr)	0.00%	0.00%	0.00%	0.00%
Cobalt (Co)	0.01%	0.00%	0.01%	0.05%
Copper (Cu)	0.03%	0.02%	0.05%	0.30%
Iron (Fe)	0.02%	0.03%	0.11%	1.20%
Lanthanum (La)	<LOQ	<LOQ	0.00%	0.00%
Lead (Pb)	<LOD	<LOD	<LOD	<LOQ
Lithium (Li)	<LOD	<LOD	<LOQ	0.01%
Magnesium (Mg)	0.00%	0.01%	0.21%	0.15%
Manganese (Mn)	<LOQ	0.00%	0.01%	0.02%
Molybdenum (Mo)	<LOD	<LOD	<LOD	<LOD
Nickel (Ni)	0.00%	0.00%	0.00%	0.02%
Phosphorus (P)	0.00%	<LOQ	0.01%	0.02%
Potassium (K)	0.01%	0.01%	0.03%	0.33%
Selenium (Se)	<LOD	<LOD	<LOD	<LOD
Silver (Ag)	<LOD	<LOD	<LOD	<LOD
Strontium (Sr)	0.00%	0.00%	0.01%	0.00%
Tellurium (Te)	<LOD	<LOD	<LOD	<LOD
Thallium (Tl)	<LOD	<LOD	<LOD	<LOD
Tin (Sn)	0.01%	0.01%	0.01%	0.09%
Titanium (Ti)	0.00%	0.00%	0.03%	0.05%
Vanadium (V)	<LOD	<LOD	0.00%	0.00%
Yttrium (Y)	0.00%	0.00%	0.00%	0.00%
Zinc (Zn)	0.00%	0.00%	0.00%	0.01%
Zirconium (Zr)	0.00%	<LOQ	0.00%	0.00%

a potential for chronic pulmonary inflammation even with materials that initially appeared to be less reactive.

BALF LDH activity and cytokines/chemokines

To further determine pulmonary cell injury, lactate dehydrogenase (LDH), a cytosolic enzyme released upon cell membrane damage, activities in BALF were measured. The universal rise in LDH activity at day 1 post-exposure across all exposure groups relative to saline controls confirms acute cellular injury induced by all tested dusts (Figure 3). This initial widespread cytotoxicity suggests a nonspecific, immediate response to particle deposition. The subsequent elevation of LDH restricted to the MS 5 group at day 21 post-exposure, and then to both MS 5 and ES A groups at day 84 post-exposure, corroborates cell differential data, indicating sustained or recurrent cytotoxicity specifically associated with these two materials. This pattern suggests that MS 5, and to a lesser extent ES A, possess properties that promote prolonged or exacerbated cellular damage.

To characterize the dust-induced pulmonary inflammation and damage, inflammatory mediators and signaling proteins, cytokines/chemokines, were determined in BALF. The cytokine/chemokine profiles in the BALF demonstrated a predominantly early and transient inflammatory response, characterized by distinct temporal patterns for different cytokines/chemokines (Figure 3). A marked and universal rise in both TNF-α, a key mediator of acute inflammation, and IL-6, a pleiotropic cytokine with both pro- and anti-inflammatory properties, was observed across all exposure groups at day 1 post-exposure. This synchronized surge in these inflammatory mediators, followed by a rapid return to baseline levels at subsequent time points, suggests a robust but self-limited innate immune response triggered by the initial dust exposure. The transient, less pronounced increases in IL-13 (observed in granite, ES A, and ES B groups) and IL-5 (noted in granite, MS 5, and ES A groups) at day 1 post-exposure may reflect contributions to specific aspects of the initial inflammatory phase, potentially related to Th2-type responses or eosinophil

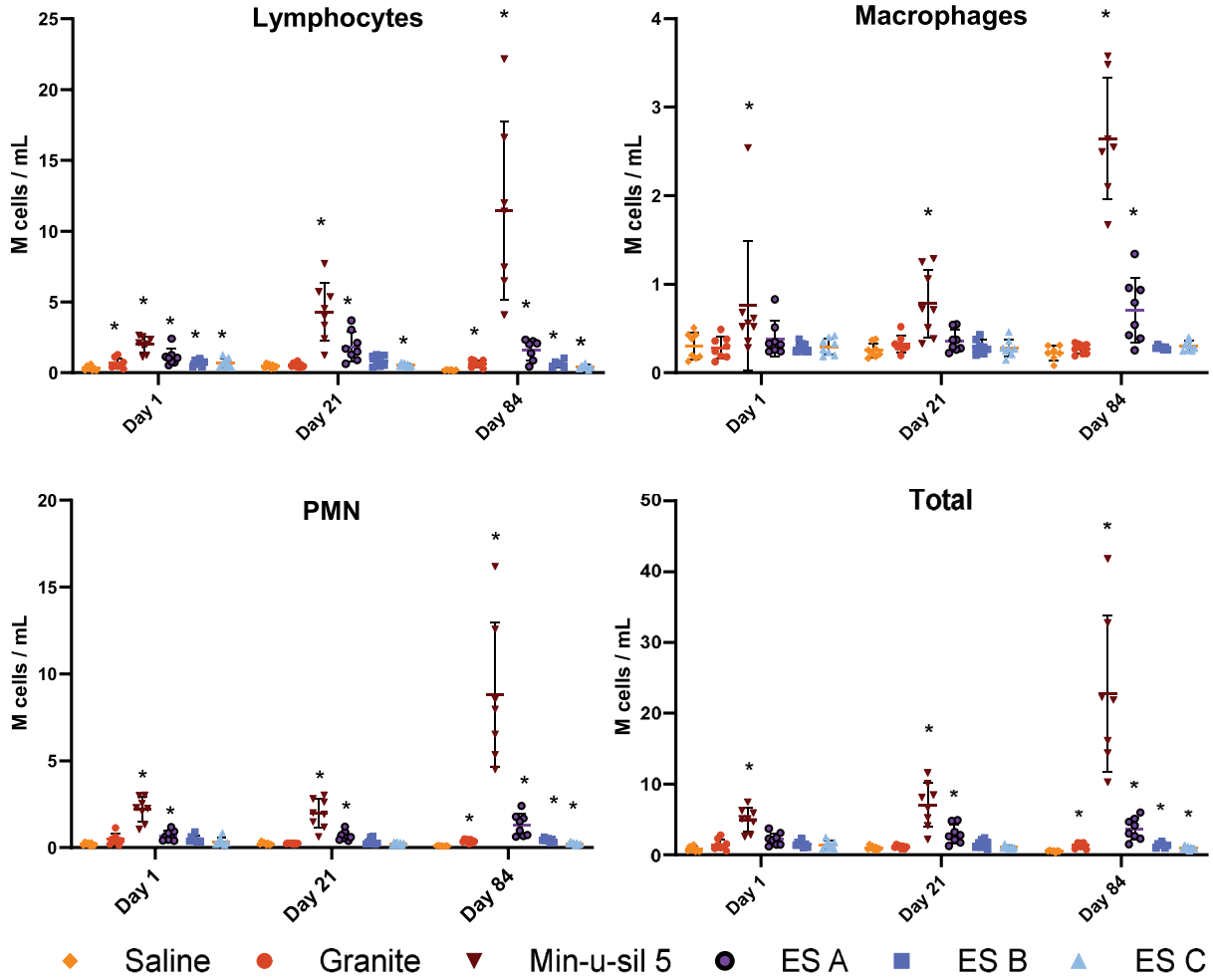

FIGURE 2. Inflammatory cell counts in bronchoalveolar lavage fluid after exposure to various particle suspensions. The graphs show cell concentrations (millions/mL) of lymphocytes, macrophages, polymorphonuclear neutrophils, and total cells at days 1, 21, and 84 postexposure. Exposure groups: saline (control), granite, MS 5, and three engineered stone types (ES A, ES B, ES C). Error bars represent standard deviations. * indicates a statistically significant difference compared to the saline control ($p < 0.05$, $n = 8$ per group. MS 5 and ES a show the largest, most persistent increases.

recruitment, respectively. Elevation of the pro-inflammatory cytokine IL-1β at day 1 post-exposure in only ES A and ES B groups suggests differential initial response to these materials. The specific and isolated rise in KC/GRO, a potent neutrophil chemoattractant, in the MS 5 group exclusively at day 21 post-exposure, is in agreement with persistent neutrophil influx found in BALF cell differentials for this group.

Notably, there was an absence of pro-fibrotic cytokines such as TNF-α, IL-1β, and IL-6 at day 84 post-exposure, despite histological evidence of fibrosis in lung tissue (Figures 4 and 5). The most likely explanation is a temporal disconnect between peak cytokine expression and manifestation of fibrosis. It is postulated that upregulation of profibrotic mediators occurred between day 21 and day 84 post-exposure, driving the fibrotic process, with cytokine levels subsequently declining by the time of day 84 post-exposure BALF collection. While this study did not measure classic late-stage fibrotic mediators like TGF-β or FGF, the robust histological findings provide clear evidence of a fibrotic outcome.

Histopathology

1 day post-exposure

Histopathological analysis was performed on lung, to include bronchus-associated lymphoid tissue (BALT), and lymph node to determine the dust-induced pulmonary damage, inflammation, and

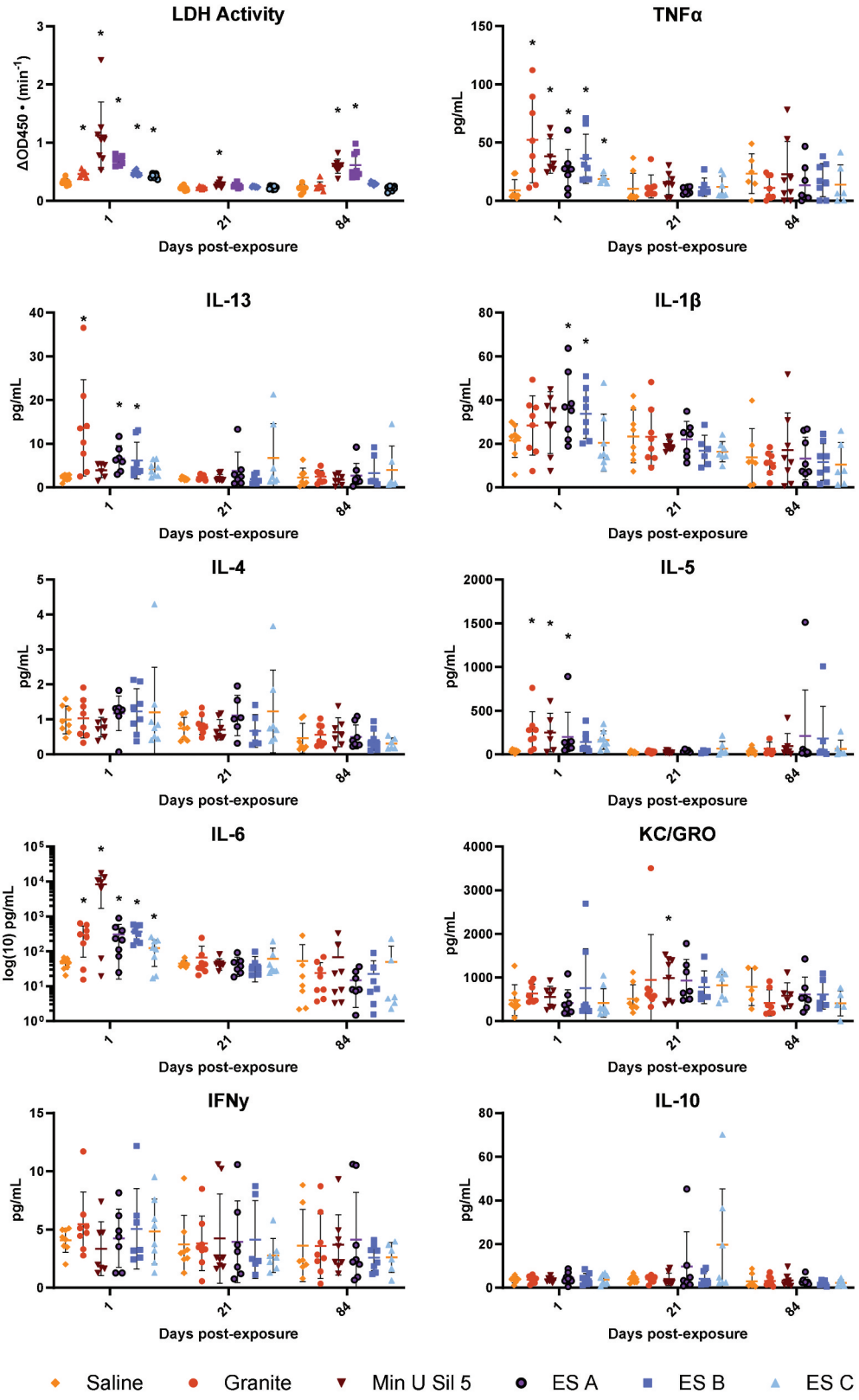

FIGURE 3. Bronchoalveolar lavage fluid (BALF) LDH activity and cytokine levels PostExposure. BALF levels of LDH activity, IFNγ, IL-10, IL-13, IL-1β, IL-4, IL-5, IL-6, KC/GRO, and TNF-α at 1-, 21-, and 84-days post-exposure to saline, granite, MS 5, ES A, ES B, and ES C. Data are presented as mean ± SD. Note that IL-6 levels are plotted on a log10 scale. * indicates statistically significant ($p < 0.05$) difference from saline control at the same time point, $n = 8$ per group.

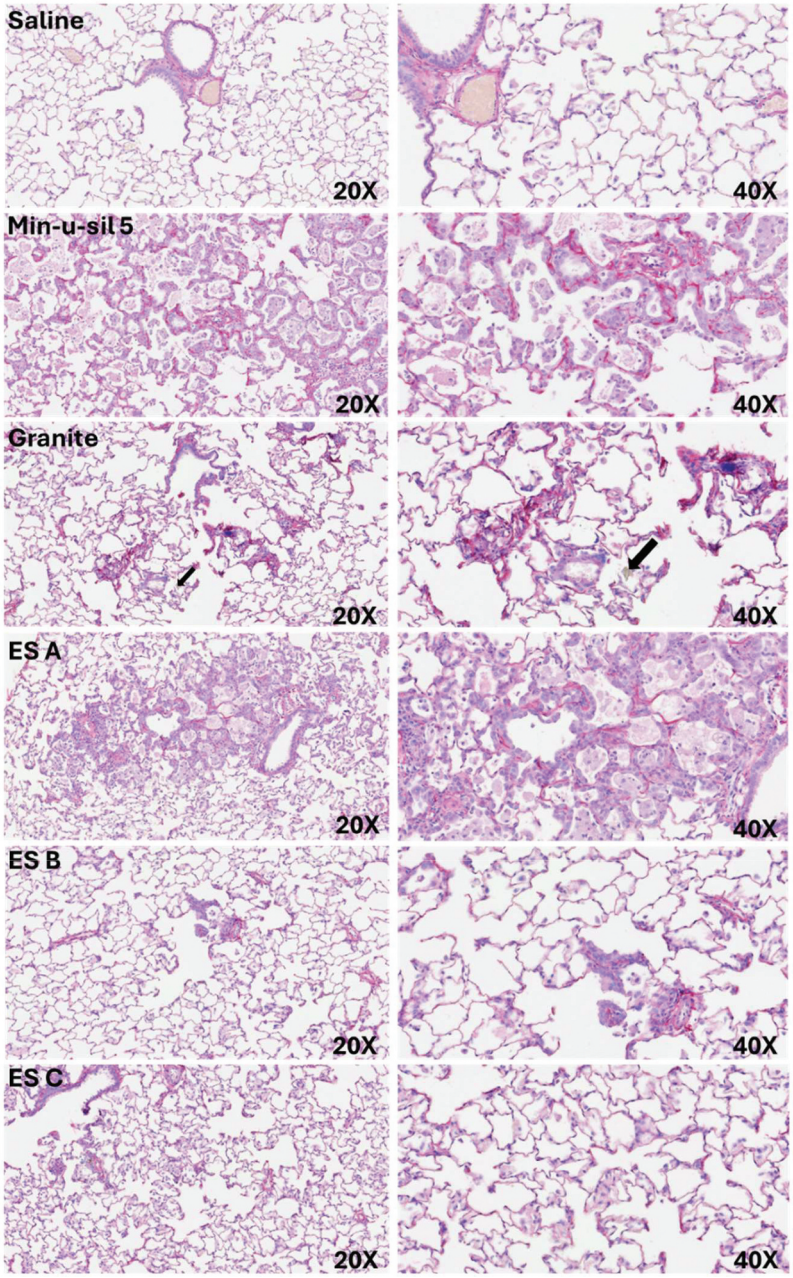

FIGURE 4. Lung tissue histopathology at 84 days post-exposure. Picrosirius red staining of lung tissue demonstrates persistent alveolitis and type II epithelial hypertrophy/hyperplasia across all exposure groups at 84 days post-exposure. Fibrosis is now evident in all groups, with greater collagen deposition (red stain) in MS 5 and ES a exposed tissues compared to granite, ES B, and ES C. Lipoproteinosis is observed in MS 5 and ES a groups. Black arrow indicates deposited foreign material.

fibrogenic responses. The average pathology/severity scores for these tissues at 1-, 21-, and 84-days post-exposure are presented in Table 3 and summarized below; the scoring system is described in the methods section.

Minimal to mild acute alveolitis (alveolar mixed cell inflammation) was present in all exposure groups, which was predominately composed of neutrophils with lesser numbers of macrophages, primarily centriacinar in distribution where the junction of the terminal bronchioles and alveolar ducts occurs, and consistently associated with type II epithelial hypertrophy/hyperplasia

Perivascular mixed cell infiltrates were present in all exposure groups; however, those exposed to

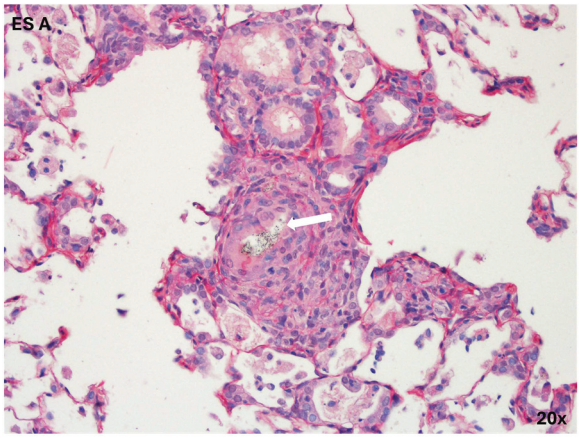

FIGURE 5. Picrosirius red staining of lung tissue post-ES a exposure. Lung tissue at 84 days post-exposure to ES A, stained with picrosirius red to visualize collagen deposition. Concentric rings of collagen are present (red) surrounding the hypertrophied epithelial cells and the foreign material (white arrow).

granite or one of the ESs exhibited increased pathology scores as compared to saline controls; infiltrates were detected in MS 5, but with similar pathology scores as saline control. There was no evidence of interstitial fibrosis or lipoproteinosis in any exposure group at this time point and there were no significant pulmonary findings in MS 5 or saline controls.

With the exception on MS 5, foreign material was found in all exposure groups. The appearance of which varied depending upon the exposure group. While no foreign material was noted in those exposed to MS 5, fine granular intra- and extracellular material was noted upon polarization of the tissue. The appearance of the foreign material in those exposed to granite, ES A, and ES B was similar and characterized by clear to light green irregular refractile globules or spicules that often-contained fine dark brown to black granulated specks. In those exposed to granite, the majority of the foreign material polarized, whereas the foreign material in those exposed to ES A and ES B often did not, though polarized material separate from the histologically noted foreign material was detected within the airways. The foreign material in those exposed to ES C consisted of larger clumps of dark brown to black non-refractile material that was less commonly associated with inflammation as compared to other exposure groups. Polarization was similar to that of ES A and ES B.

Minimal lymphoid hyperplasia as evidenced by increased lymphoid cellularity of the BALT in the lung was present in one animal exposed to ES B. In the lymph node, minimal to mild mixed cell infiltrates

TABLE 3. Average Pathology/Severity Scores in Lung Tissue (Scoring System Described in Methods), BALT, and Lymph Nodes Following Exposure to Saline, min-U-Sil 5, Granite, and Engineered Stone (ES A, ES B, ES C) at 1, 21, and 84 Days Post-Exposure. Red Color Indicates Magnitude of Severity

Average Pathology/Severity Scores															
Group	Min-u-Sil			Granite			ES A			ES B			ES C		
Post Exposure Day	1	21	84	1	21	84	1	21	84	1	21	84	1	21	84
Lung - H&E No. Examined	8	8	8	8	8	8	8	8	8	8	8	8	8	8	8
Inflammation, Mixed Cell, Alveolar	5.125	5.625	6.875	3.25	3.125	3.375	3.875	5.375	5.625	3.5	3.375	2.625	3.125	3	2.375
Cellular Aggregates/Granulomas, Alveolar	-	2.125	4.125	-	2.375	2.125	-	4.125	2.375	-	3	1	-	3	1.625
Hypertrophy/Hyperplasia	4.625	5	5.5	3.125	2	3	3.5	3.875	5.25	3.5	2.625	2.5	2.5	1.75	1.25
Lipoproteinosis, Alveolar	-	4.625	5.75	-	0.25	-	-	4	3.125	-	-	-	-	-	-
Foreign Material, Alveolar	-	-	-	3.375	3.125	3	4.375	4.5	2.875	4.125	3	2.875	4.375	4	2.25
Polarized Material, Alveolar	4.25	4.375	4.625	3.5	3.875	3.5	3.5	3.25	3	3.625	3.375	2.875	1.75	2.25	1.5
Fibrosis, Interstitial	-	1	5.375	-	-	2	-	2.625	4.125	-	-	1	-	-	1.25
Infiltrate, Mononuclear Cell, Perivascular	-	2	0.375	-	-	-	-	-	-	-	-	-	-	-	-
Infiltrate, Mixed Cell, Perivascular	1.625	1	-	3.625	-	-	4.25	-	-	3.875	-	-	4.125	0.375	-
Lung - Picrosirius Red No. Examined	8	8	8	8	8	8	8	8	8	8	8	8	8	8	8
Fibrosis, Interstitial	-	1	5.375	-	-	2	-	2.625	4.125	-	-	1	-	-	1.25
BALT - H&E No. Examined	5	5	7	7	6	8	8	5	6	8	6	7	8	6	6
Inflammation, Granulomatous	-	-	1.571	-	-	-	-	-	0.833	-	-	0.286	-	-	0.333
Increased Cellularity, Lymphocytes	-	0.2	0.429	-	0.167	-	-	-	-	0.125	-	-	-	-	0.167
Polarized Material	-	0.2	0.571	-	-	-	-	0.4	0.333	-	-	0.143	-	-	0.167
Lymph Node - H&E No. Examined	8	8	6	5	7	8	8	8	7	5	8	8	7	7	7
Infiltrate, Mixed Cell	1.375	-	-	0.4	-	-	1.125	-	-	1.2	-	-	1	-	-
Inflammation, Granulomatous	-	2	3.667	-	-	1.25	-	0.875	3.571	-	-	1.75	-	-	1
Cellularity, Increased, Lymphocytes	0.125	1.875	0.833	0.2	0.714	0.75	0.125	1.5	1.143	-	0.625	0.375	-	0.571	0.429
Polarized Material	-	1.375	2.333	-	-	0.875	-	0.625	1.143	-	-	1	-	-	0.857
Fibrosis	-	-	2.167	-	-	-	-	-	0.714	-	-	-	-	-	-

composed of foamy macrophages and neutrophils were noted in all exposure groups. Neutrophils were predominately present in the sinuses while macrophages expanded the paracortex and medullary cords. Minimal lymphoid hyperplasia was also present in those exposed to MS 5, granite, and ES A. There were no significant lymphoid findings in the saline controls. In general, the greatest pathology scores were noted in those exposed to MS 5 and, to a lesser extent, ES A, with those exposed to ES C having the lowest pathology scores.

21-days post-exposure

Alveolitis and type II epithelial hypertrophy/hyperplasia were still present in all exposure groups with a rise in pathology scores in those exposed to MS 5 and ES A and a slight fall in pathology scores in those exposed to granite, ES B, and ES C, as compared to 1-day post-exposure scores (Table 3). Inflammation had transitioned and was now predominately composed of macrophages, with significantly less numbers of neutrophils as compared to 1-day post-exposure. In addition, discrete aggregates of cells and/or early granulomas were noted. Foreign material was still detected in the exposure groups in which it had been present at 1-Day post-exposure, with a reduction in pathology scores as compared to 1-Day Post Exposure scores in all groups except ES A, in which there was a slight rise in score. This increase correlated with an enhanced pathology score for the presence of cellular aggregates/granulomas in ES A, as compared to other exposure groups. Lipoproteinosis now occurred in those exposed to MS 5, ES A, and to lesser degree, granite. In addition, interstitial fibrosis, as highlighted by picrosirius red staining, began to develop in those exposed to MS 5 and ES A. Polarized material was still present in all exposure groups with a slight increase in pathology scores in those exposed to MS 5, granite, and ES C and a slight reduction in those exposed to ES A and ES B, as compared to 1-day post-exposure scores. The presence of perivascular mixed cell infiltrates had resolved in all groups to within the normal range of variation. There were no significant pulmonary findings in saline controls.

In the BALT, polarized material was found in those exposed to MS 5 and ES A and minimal lymphoid hyperplasia was present in one animal exposed to MS 5.

In the lymph node, mixed cell infiltration had resolved but granulomatous inflammation was now present in those exposed to MS 5 and, to a lesser extent, ES A. Lymphoid hyperplasia was detected in all groups, including saline controls; however, severity was higher than that of controls in all exposed groups except ES C, in which a similar response to that of saline controls was found. Polarized material was present in those exposed to MS 5 and ES A. In general, the greatest pathology scores were noted in those exposed to MS 5 and, to a lesser extent, ES A, with those exposed to ES C having the lowest pathology scores.

84-DaysPpost-exposure

Alveolitis, cellular aggregates/granulomas, and type II epithelial hypertrophy/hyperplasia were still present in all exposure groups (Table 3). Similar to trends noted at 21-days post-exposure, there was a continual rise in pathology scores in those exposed to MS 5 and ES A and a decrease in pathology scores in those exposed to ES B and ES C. Interestingly, there was a rebound in those exposed to granite, with a slight elevation in pathology scores for these findings as compared to 21-days post-exposure. Interstitial fibrosis was now present in all exposure groups but to a lesser extent in granite, ES B, and ES C as compared to MS 5 and ES A (Figure 4). There was progression of fibrosis in MS 5 and ES A at this time point as compared to 21-days post-exposure. Lipoproteinosis was only present in those exposed to MS 5 and ES A and was no longer noted in those exposed to granite. Pathology scores increased in those exposed to MS 5 and ES A, as compared to 21-days post-exposure. Except for MS 5, foreign material was still present in all exposure groups (Figure 5), but with reduced pathology scores as compared to 21-days post-exposure. Polarized material was still found in all exposure groups with a slight increase in pathology scores in those exposed to MS 5 and reduction in the others, as compared to 21-days post exposure. There were no significant pulmonary findings in saline controls.

In the BALT, polarized material and granulomatous inflammation were now present in all exposure groups except granite, with MS 5 and ES A exhibiting increased severity as compared to ES B and ES C. Lymphoid hyperplasia was still present in those exposed to MS 5 with an elevation in

severity as compared to 21-days post-exposure and was present in one animal exposed to ES B.

In the lymph node, granulomatous inflammation and polarized material were now present in all exposure groups (Figure 6), with increased severity in those exposed to MS 5 and ES A, as compared to other exposure groups and to findings at 21-days post-exposure. Fibrosis was now noted in those exposed to MS 5 and, to a lesser extent, ES A. Lymphoid hyperplasia was found in all groups, including saline controls; however, severity was higher than that of controls in all exposed groups except ES B and ES C, in which it was considered within the range of normal variation. In general,

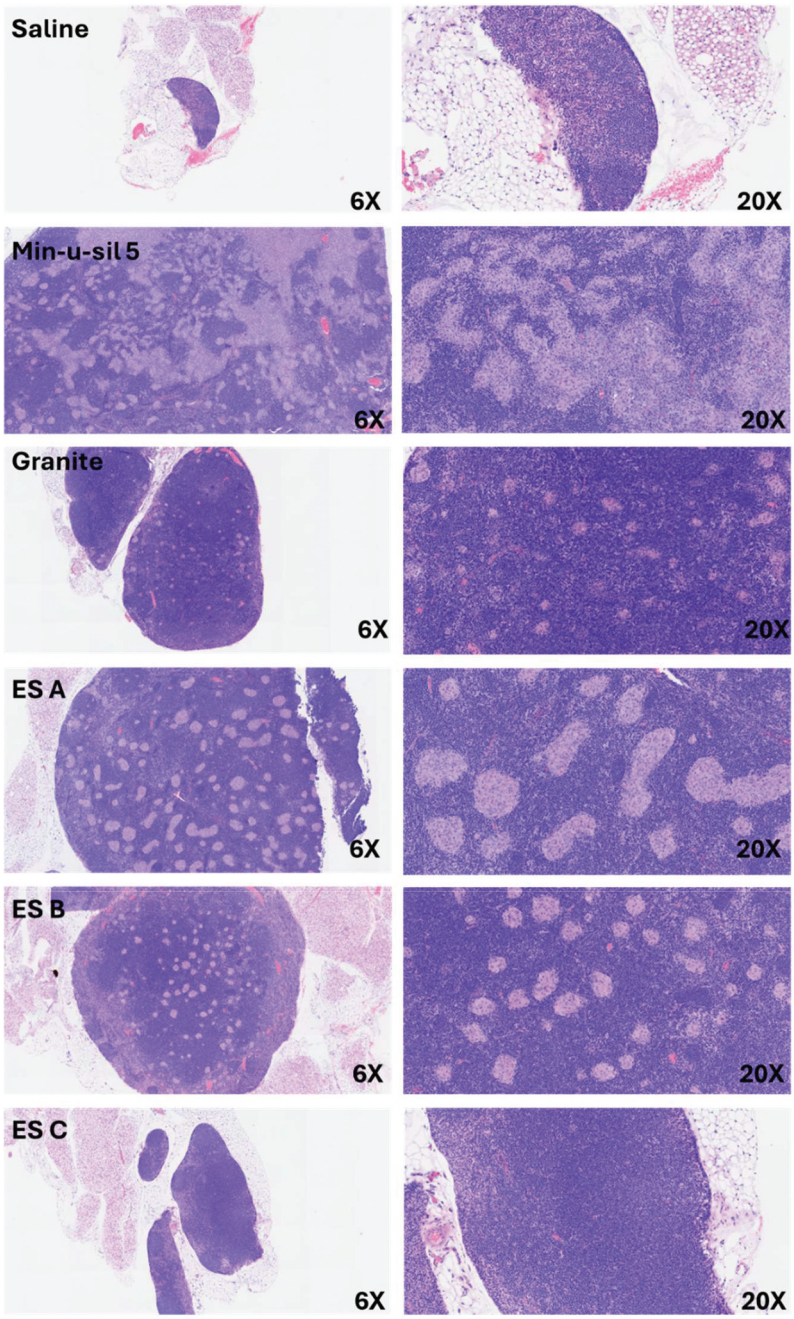

FIGURE 6. Tracheobronchial lymph node histopathology at 84 days post-exposure. representative images of lymph tissue. Tissues were stained with hematoxylin and eosin (H&E). Magnifications are indicated on the images (6X and 20X). At 84 days post-exposure, polarized material and granulomatous inflammation were present in the lymph tissue of all exposure groups except granite. MIN-U-SIL 5 and ES a exhibited increased severity of these findings compared to ES B and ES C. Lymphoid hyperplasia was observed in the MIN-U-SIL 5 exposed group, with increased severity.

the greatest pathology scores were noted in those exposed to MS 5 and, to a lesser extent, ES A, with those exposed to ES C displaying the lowest pathology scores.

Hematology

To explore Engineered Stone Dust (ESD)-induced systemic toxicity, hematology was performed. MS 5 exposure resulted in sustained neutrophilia, early hyperglycemia, and late reticulocytosis (Tables 4 and 5). Granite exposure led to no significant CBC changes but produced increased globulin at day 21 and elevated alanine aminotransferase (ALT) at day 84 post-exposure. ES A exposure induced neutrophilia and hyperglycemia at earlier time points, along with changes in red blood cell (RBC) size distribution (RDW-SD) and platelet parameters (MPV, P-LCR), as well as decreased phosphorus and amylase at day 84 post-exposure. ES B exposure resulted in minimal CBC changes, with only a transient fall in platelet size variation (PDW-SD), but also initiated elevated ALT at day 84 post-exposure, similar to granite. ES C exposure produced the fewest changes, with a transient reduction in BUN at day 21 post-exposure and a late decrease in MPV and P-LCR. There appears to be variation in the biological effects of the different dusts, with MS 5 showing the most pronounced and persistent changes, ES A exhibiting a distinct pattern of inflammation and effects on RBC and platelets, and ES B and ES C displaying relatively fewer effects, although ES B shared the delayed ALT rise with granite. In summary, exposure to various dusts revealed distinct hematological and biochemical profiles over 84 days, with MS 5 inducing the most persistent inflammation and RBC changes, ES A inducing inflammation with unique platelet effects, granite and ES B eliciting delayed liver enzyme elevations despite minimal initial impact, and ES C showing the least biological activity.

Linear regression analysis

Our statistical analysis explored the relationship between stone composition and the observed biological effects. While linear regression confirmed that the % CS was a significant predictor for many key endpoints, including inflammatory cell influx in BALF and changes in blood parameters, it did not account for all the observed variability. Principal Component Analysis (PCA) revealed high multicollinearity between several trace metals (Supplemental Figure S1), making it difficult to isolate the independent effect of each element. However, further modeling consistently showed that the inclusion of certain trace metals (such as Al, Co, and Fe) in conjunction with silica significantly improved the model's ability to predict toxicity endpoints compared to silica alone. This finding suggests that while silica is the primary pathogenic component, the unique mixture of trace metals in each type of stone acts as a significant contributor to overall toxic potential. This is in agreement with recent *in vitro* observations which reported that metals like Al and Co were significantly associated with macrophage toxicity, independent of silica content.

Discussion

This study is the first to demonstrate *in vivo* utilizing IT instillation in rats that dust from ES induced progressive lung disease. The high CS content of ES A and pure silica control (MS 5) initiated a marked and persistent inflammatory response, with an acute spike in pro-inflammatory cytokines such as IL-1β suggesting that inflammasome activation is a key early event in the observed pathology (van de Veerdonk et al. 2011). This initial inflammation and cellular injury progressed to significant tissue damage by day 84, manifesting as severe fibrosis and granulomatous inflammation in both the lungs and lymph nodes. Critically, the fibrotic damage continued to worsen long after the initial exposure, demonstrating a self-perpetuating disease process that is a hallmark of silica-induced pathology (Porter et al. 2004). Beyond the lungs, these high-silica dusts also produced significant systemic effects, including sustained changes in blood cell counts. In contrast, dust from granite and lower-silica ES produced milder, more transient lung inflammation. The difference in fibrogenicity between ES A and other ES materials may be attributable to its composition. ES A's high CS content is the most probable initiator of severe effects. Conversely, the lower silica content of ES B and C, combined with a different profile of trace metals,

TABLE 4. Complete Blood Count. Values are means ± SD. * indicates significant difference ($p < 0.05$) from control. For visual clarity, measured parameters where no significant difference from control at any time point were observed have been excluded from this table.

Treatment	Day	Hct (%)	Mchc (G/dl)	Rdw-sd (Fl)	Ret# (K/ul)	Pdw (Fl)	Mpv (Fl)	P-lcr (%)	Wbc (K/ul)	Neut# (K/ul)	Lymph# (K/ul)	Neut%	Lymph%
Control	1	41 ± 5	32.7 ± 1.0	30.3 ± 2.0	360 ± 50	7.9 ± 0.6	7.0 ± 0.4	6.4 ± 2.3	5.9 ± 1.9	1.07 ± 0.44	4.5 ± 1.4	17.5 ± 3.7	76 ± 5
	21	43.3 ± 2.6	34.0 ± 1.0	28.7 ± 0.6	264 ± 37	8.8 ± 0.3	7.45 ± 0.19	8.6 ± 1.1	8.0 ± 1.8	0.76 ± 0.25	7.0 ± 1.4	9.4 ± 1.3	87.2 ± 2.2
	84	42 ± 6	33.6 ± 1.4	29.7 ± 1.9	210 ± 30	8.3 ± 0.5	7.0 ± 0.2	6.6 ± 0.9	4.5 ± 0.6	0.77 ± 0.31	3.4 ± 0.4	17 ± 6	76 ± 8
Min u Sil 5	1	44.3* ± 1.8	31.7* ± 0.9	32.0 ± 1.7	410 ± 40	8.1 ± 0.7	7.2 ± 0.4	7.7 ± 2.7	7.2 ± 1.0	1.71* ± 0.13	4.9 ± 0.9	23.9* ± 3.1	68 ± 4
	21	43.9 ± 2.6	34.0 ± 0.6	29.2 ± 1.2	270 ± 14	8.9 ± 0.5	7.6 ± 0.3	9.5 ± 1.7	8.3 ± 1.6	1.32* ± 0.27	6.6 ± 1.5	16.2* ± 3.3	78.5* ± 4.0
	84	44.9 ± 2.8	33.0 ± 1.1	30.3 ± 2.2	248* ± 32	8.0 ± 0.8	6.9 ± 0.4	6.0 ± 2.2	4.9 ± 1.0	1.40* ± 0.41	3.2 ± 0.9	29 ± 8	65* ± 9
Granite	1	39.5 ± 5.6	32.5 ± 0.7	30.5 ± 1.4	360 ± 40	7.8 ± 0.6	6.8 ± 0.4	5.9 ± 1.8	5.7 ± 2.2	1.3 ± 0.6	4.0 ± 1.4	22 ± 5	71 ± 7
	21	42.9 ± 1.8	34.1 ± 0.5	29.3 ± 0.9	262 ± 28	8.5 ± 0.4	7.35 ± 0.24	8.1 ± 1.3	7.3 ± 2.1	0.86 ± 0.19	6.1 ± 2.0	12.6 ± 4.3	82.7 ± 6.5
	84	44.6 ± 2.3	32.9 ± 1.2	30.5 ± 2.0	229 ± 13	8.1 ± 0.6	6.9 ± 0.3	6.0 ± 1.7	4.8 ± 0.8	1.02 ± 0.30	3.4 ± 0.6	21.0 ± 4.1	71.5 ± 6.4
ES A	1	43.1 ± 3.1	32.2 ± 1.2	31* ± 2	360 ± 50	7.6 ± 0.4	6.9 ± 0.3	6.7 ± 2.3	6.7 ± 1.3	1.08 ± 0.33	5.1 ± 1.0	16.0 ± 2.6	76.6 ± 3.7
	21	45.1 ± 2.2	33.4 ± 0.7	30.2* ± 1.0	290 ± 30	8.7 ± 0.6	7.6* ± 0.5	9.7* ± 3.2	9.7* ± 0.6	1.30* ± 0.17	8.0* ± 0.5	13.4* ± 1.6	82.6* ± 1.8
	84	43.2 ± 3.5	33.7 ± 1.6	29.7 ± 2.7	220 ± 30	7.8 ± 0.4	6.6* ± 0.3	4.5* ± 1.1	4.3 ± 0.9	0.72 ± 0.22	3.2 ± 0.7	17 ± 4	76 ± 4
ES B	1	42.0 ± 3.9	32.5 ± 0.8	30.4 ± 1.0	380 ± 41	8.0* ± 0.3	7.0 ± 0.3	6.4 ± 1.7	6.8 ± 2.4	1.3 ± 0.5	5.1 ± 2.0	19 ± 4	75 ± 5
	21	44.3 ± 2.4	33.7 ± 0.9	29.7 ± 1.4	261 ± 20	8.2* ± 0.5	7.3 ± 0.4	8.3 ± 2.2	9.0 ± 1.1	0.92 ± 0.21	7.7 ± 1.0	10.2 ± 2.2	85.4 ± 3.3
	84	43.9 ± 1.4	33.2 ± 0.5	30.3 ± 1.8	216 ± 21	7.9 ± 0.5	6.8 ± 0.4	5.5 ± 2.2	5.0 ± 1.0	1.01 ± 0.39	3.7 ± 0.6	20 ± 6	74 ± 6
ES C	1	44.2 ± 3.4	32.1 ± 0.6	30.0 ± 1.2	400 ± 40	7.9 ± 0.5	6.9 ± 0.3	6.1 ± 1.4	6.5 ± 2.0	1.09 ± 0.46	4.9 ± 1.5	16.8 ± 4.2	76 ± 6
	21	44.1 ± 2.2	33.8 ± 0.9	29.7 ± 2.0	266 ± 43	8.5 ± 0.5	7.3 ± 0.4	7.6 ± 2.0	7.2 ± 2.6	0.71 ± 0.26	6.2 ± 2.3	10.1 ± 2.7	85.1 ± 4.1
	84	46.5 ± 3.9	32.6 ± 0.5	30.9 ± 1.6	230 ± 30	7.9 ± 0.4	6.8* ± 0.2	5.0* ± 0.8	5.0 ± 1.0	0.69 ± 0.22	3.9 ± 0.9	14.1 ± 4.4	78 ± 6

TABLE 5. Serum Chemistry. Values are means ± SD. * indicates significant difference ($p < 0.05$) from control.

Group	Time (Days)	Glucose (Glu)	Creatinine (Crea)	Blood Urea Nitrogen (Bun)	Phosphorus (Phos)	Globulin (Glob)	Alb/glob Ratio	Alanine Aminotransferase (Alt)	Amylase (Amyl)
Control	1	171.75 ± 65.95	0.19 ± 0.14	15.75 ± 1.67	11.10 ± 1.84	2.53 ± 0.35	1.49 ± 0.24	109.88 ± 37.82	1377.63 ± 211.45
	21	216.25 ± 68.01	0.19 ± 0.14	17.13 ± 1.46	8.40 ± 1.37	2.29 ± 0.16	1.56 ± 0.30	98.38 ± 36.01	1005.00 ± 110.72
	84	186.43 ± 55.86	0.54 ± 0.05	18.57 ± 1.99	6.50 ± 0.61	2.77 ± 0.20	1.18 ± 0.16	83.57 ± 10.72	1380.29 ± 47.66
Min u Sil 5	1	258.13* ± 51.90	0.31 ± 0.16	17.38 ± 1.69	11.41 ± 1.85	2.55 ± 0.30	1.39 ± 0.23	125.88 ± 29.03	1311.75 ± 58.37
	21	233.38 ± 92.53	0.24 ± 0.17	17.50 ± 0.93	8.24 ± 0.53	2.26 ± 0.16	1.45 ± 0.18	85.75 ± 10.78	1053.38 ± 153.06
	84	194.50 ± 64.13	0.51 ± 0.14	19.00 ± 0.82	5.81 ± 1.04	2.70 ± 0.21	1.27 ± 0.14	107.50 ± 45.14	1280.38 ± 221.14
Granite	1	196.13 ± 63.90	0.18 ± 0.10	17.13 ± 2.03	110.36 ± 281.89	2.26 ± 0.37	1.65 ± 0.61	102.13 ± 24.18	1467.00 ± 163.59
	21	210.75 ± 45.48	0.19 ± 0.14	16.63 ± 2.50	8.45 ± 0.56	2.45* ± 0.17	1.30 ± 0.13	99.75 ± 30.03	1039.63 ± 87.57
	84	202.38 ± 53.58	0.53 ± 0.18	19.63 ± 1.06	6.04 ± 1.37	2.79 ± 0.12	1.18 ± 0.09	103.00* ± 19.12	1386.38 ± 144.83
ES A	1	243.25* ± 61.62	0.25 ± 0.19	15.50 ± 2.78	10.55 ± 1.48	2.50 ± 0.22	1.31 ± 0.18	93.25 ± 18.42	1386.00 ± 144.06
	21	243.63 ± 71.35	0.12 ± 0.05	17.00 ± 1.07	8.73 ± 0.49	2.41 ± 0.16	1.33 ± 0.15	90.13 ± 11.67	1109.25 ± 116.70
	84	187.75 ± 74.33	0.43 ± 0.21	17.38 ± 0.92	5.63* ± 0.47	2.75 ± 0.19	1.25 ± 0.23	77.13 ± 14.78	1224.00* ± 173.77
ES B	1	240.00 ± 107.17	0.21 ± 0.16	15.75 ± 1.49	10.18 ± 1.02	2.56 ± 0.31	1.29 ± 0.18	110.13 ± 33.71	1448.25 ± 163.55
	21	208.50 ± 67.79	0.15 ± 0.05	16.25 ± 1.49	8.88 ± 0.48	2.47 ± 0.19	1.26* ± 0.15	100.63 ± 29.59	1050.00 ± 146.60
	84	204.63 ± 62.73	0.46 ± 0.11	20.13 ± 2.03	5.90 ± 0.55	2.91 ± 0.29	1.14 ± 0.21	93.88* ± 11.52	1326.25 ± 137.54
ES C	1	236.13 ± 57.28	0.16 ± 0.11	14.88 ± 2.47	9.85 ± 0.64	2.59 ± 0.29	1.26 ± 0.24	104.50 ± 20.87	1501.00 ± 177.88
	21	206.13 ± 58.16	0.18 ± 0.14	15.25* ± 1.49	8.93 ± 0.71	2.50 ± 0.36	1.39 ± 0.41	98.00 ± 23.18	993.63 ± 177.85
	84	229.75 ± 82.75	0.46 ± 0.17	19.63 ± 2.13	6.40 ± 0.41	2.84 ± 0.21	1.15 ± 0.19	96.00 ± 24.55	1386.38 ± 196.40

might account for significantly reduced fibrogenic potential.

Linear regression analysis examined the relationship between % silica and trace metals with the measured health endpoints. Silica content was significantly associated with several BALF and blood parameters, some positively (inflammatory cells and cytokines) and some negatively (GGT and cholesterol). Analysis of trace metals also revealed significant associations with various endpoints. Importantly, models incorporating both silica and a single trace metal often explained more of the variation in the measured outcomes than models with silica alone. Data suggest that the toxicity of ESD is not solely due to silica but may also be significantly influenced by the presence and interaction of various trace metals.

A recent *in vitro* investigation employing a comprehensive panel of ES dusts ($n > 50$) noted that while the RCS content was a significant predictor of cytotoxicity, other inorganic constituents, particularly Co and Al, exhibited comparable or greater influence. Further, Ramkissoon et al. (2024) demonstrated that even ES formulations designed with reduced CS content elicited marked inflammatory responses in exposed cells. Pavan et al. (2016) examined the fibrotic potential of ESD in an *in vitro* human lung epithelial model (BEAS-2B). All tested artificial stone dust samples, irrespective of resin presence, induced EMT. Notably, pre-treatments designed to expose free quartz surfaces (heating) or enhanced particle reactivity (heating followed by grinding) did not markedly alter the EMT response compared to untreated dust. EMT plays a critical role in driving the fibrotic cascade in silicosis primarily by contributing to the pool of myofibroblasts, cells responsible for excessive production of extracellular matrix (ECM). Epithelial cells that undergo EMT lose their epithelial identity and acquire mesenchymal characteristics, transforming into myofibroblasts (Li et al. 2016). These myofibroblasts are characterized by their enhanced ability to synthesize and secrete ECM components, including various types of collagens, which are the predominant structural proteins of fibrotic tissue. This overproduction and deposition of ECM in lung interstitium leads to thickening and stiffening of lung tissue, a hallmark of pulmonary fibrosis in silicosis (Stone et al. 2016).

Both the present study and Ramkissoon et al. (2024) demonstrated that the toxicity attributed to stone dust is not solely due to CS; trace metals also play a significant role in inducing lung injury and inflammation. Ramkissoon et al. (2024) found high variability in the non-silica elemental composition of ES samples and identified metals including Ti, Cu, Co, and Fe within the ultrafine particles generated from cutting. While CS content was associated with macrophage inflammatory response, Co and Al were associated with macrophage toxicity. Ramkissoon et al. (2024) reinforced the importance of these trace metals by showing that even reduced-silica ES and non-ES materials might induce marked inflammatory responses. Overall, these studies converge on the finding that trace metals, especially Co and Al, are

significantly associated with adverse lung cell responses, suggesting that the toxicity of stone dust is a result of both CS and trace metals. Despite these findings, our analysis faced methodological limitations, primarily due to multicollinearity among several metals. The observed multicollinearity may lead to less reliable statistical inference in more complex multiple linear regression models, making attempts to isolate the individual contributions of each metal challenging. Although our models frequently identified several trace metals as significant predictors, the issue of multicollinearity warrants caution when interpreting the specific roles and relative importance of each metal.

Silicosis, a debilitating occupational lung disease, results from the interaction between inhaled RCS particles and the immune system (Pollard 2016). Particles less than 5 μm in diameter are able to reach the alveolar spaces, triggering a robust inflammatory response (Porter et al. 2004). Macrophages attempt to engulf and clear the silica; however, their persistent presence overwhelms this phagocytic capacity, resulting in prolonged inflammation and release of pro-inflammatory cytokines and reactive oxygen species (ROS) (Porter et al. 2002; Vallyathan et al. 1995). These mediators exacerbate the inflammatory milieu. Cytokines recruit additional immune cells, including fibroblasts, responsible for collagen production, a key component of scar tissue (She, Yu, and Tang 2021). Concurrently ROS directly damage lung tissue and contribute to oxidative stress, further fueling inflammation (Thibodeau et al. 2004; Vallyathan et al. 1988). The hallmark feature of silicosis, fibrosis, results from this excessive collagen deposition, progressively thickening and stiffening the lungs, thereby compromising gas exchange and lung function. Emerging evidence suggests additional mechanisms at play. RCS particles may directly injure airway epithelial cells (Wu et al. 2020), contributing to tissue damage. Komai et al. (2019) suggested a role for EMT, where epithelial cells transform into scar-forming fibroblasts under the influence of silica. Multiple factors contribute to lung tissue injury in silicosis, indicating the complex pathogenesis of this disease.

ES-associated silicosis presents as a distinct clinical entity within the spectrum of silicosis, characterized by a significantly lower exposure threshold and reduced latency period compared to classical forms of the disease (Ramkissoon, Gaskin, Thredgold, et al. 2022). This accelerated disease trajectory, frequently detected in younger individuals with comparatively limited cumulative silica exposure, differentiates ES-associated silicosis from classic silicosis typically associated with occupations such as hard-rock mining and sandblasting. Rose et al. (2019) reported only 18 US cases with two fatalities, while Fazio et al. (2023) noted 52 California cases with 10 fatalities among immigrant workers, raising concerns for underreporting among this transient population. Mandatory medical surveillance in Australian states like Victoria and Queensland identified a high silicosis burden, with nearly a quarter of over 1,800 screened workers affected, and 15% progressing to severe progressive massive fibrosis (Hoy et al. 2023) In contrast to Fazio et al. (2023), Hoy et al. (2023) findings indicate serious adverse health consequences. Studies in Italy (54.5% prevalence) (Pascual et al. 2010), Israel (Kramer et al. 2012), Spain (Perez-Alonso et al. 2014), and Belgium (Ronsmans et al. 2018) also reported outbreaks. Washington State workplace inspections revealed that 9 out of 18 shops exceeded OSHA's RCS Permissible Exposure Limit (PEL) (Lofgren 2008), supported by a significant rise in OSHA citations for PEL exceedances at stone countertop sites (from 4 annually in 2000–2002 to 59 in 2003–2011), suggesting inadequate dust control measures (Qi and Echt 2016).

Limitations

While the present investigation provides critical insights into the effects of IT instillation ESD exposure on lung tissue, several critical limitations must be noted. First, it should be noted that the particle samples used in this study were not freshly generated and thus do not fully recapitulate the exposure conditions that ES workers may face. The primary hazard of ES arises from freshly fractured RCS generated during fabrication processes. Aged samples have undergone surface changes, including hydration and adsorption, which significantly reduce their reactivity and, consequently, toxicity. The most critical events in development of silicosis occur immediately after exposure to freshly fractured RCS (Castranova et al. 2002). These initial events involve the rapid generation of ROS (Vallyathan et al. 1995), lipid peroxidation

(Vallyathan et al. 1988), DNA fragmentation (Thibodeau et al. 2004), and activation of multiple inflammatory pathways (Fubini and Hubbard 2003, Hornung et al. 2008). In addition, the dust samples used in this study lack VOC's that may be generated during machining (Ramkissoon, Gaskin, Hall, et al. 2022) and suspension in PBS may alter surface chemistry. Second, the initial phase of our investigation into the toxicity induced by ESD, utilized IT installation due to its greater flexibility and deposition efficiency compared to inhalation exposure. However, due to the numerous drawbacks associated with IT including bolus effect, high artificial excess deposition of chemical, methodological use of anesthetic altering physiological pulmonary elimination of contaminants may account for the induced inflammatory and fibrotic responses (Kacew and Demir 2025). Although the dose rate and distribution of particles in lungs are different between IT and whole-body inhalation exposures, Driscoll et al. (2000) stated inhalation exposure is the "natural route of entry of substances" into the host and preferred method for introduction of toxicants into the lungs. It is noteworthy that IT instillation of humidifier chemicals into the lungs produced pulmonary inflammation, altered histopathological abnormal blood cell counts, which were not seen following inhalation exposure (Kacew and Demir 2025). Hence both exposure methods might not generate similar results of pulmonary inflammation, fibrosis, and immune responses (Driscoll et al. 2000). Subsequent research needs to involve inhalation exposure studies to more accurately assess the combined influence of inhalation dynamics, size distribution, aging, and VOCs of particles deposited throughout the respiratory tract.

Conclusions

Unresolved questions regarding the interaction between RCS and other emissions components, and specific pathological pathways leading to accelerated silicosis, require further investigation. Determining these mechanisms is critical for development of effective mitigation strategies to safeguard workers in the stone countertop industry from suffering detrimental health consequences due to RCS exposure. Ultimately, this study demonstrates that ESD administered IT poses a significant and complex health risk, driven not only by silica but also by trace metal content, emphasizing the need for further research especially the use of inhalation into the mechanisms underlying accelerated silicosis.

Disclosure statement

No potential conflict of interest was reported by the author(s).

Funding

The author(s) reported there is no funding associated with the work featured in this article.

Data availability statement

The data that support the findings of this study are available from the corresponding author, WKM, upon reasonable request.

Disclaimer

The findings and conclusions in this report are those of the author(s) and do not necessarily represent the official position of the National Institute for Occupational Safety and Health (NIOSH), Centers for Disease Control and Prevention (CDC). Mention of any company or product does not constitute endorsement by NIOSH/CDC.

References

Anlar, H. G., M. Bacanli, S. İritaş, C. Bal, T. Kurt, E. Tutkun, O. Hinc Yilmaz, and N. Basaran. 2017. "Effects of Occupational Silica Exposure on Oxidative Stress and Immune System Parameters in Ceramic Workers in Turkey." *Journal of Toxicology & Environmental Health A* 80 (13–15): 688–696. https://doi.org/10.1080/15287394.2017.1286923.

Blackford, J. A., W. Jones, R. D. Dey, and V. Castranova. 1997. "Comparison of Inducible Nitric Oxide Synthase Gene Expression and Lung Inflammation Following Intratracheal Instillation of Silica, Coal, Carbonyl Iron, or Titanium Dioxide in Rats." *Journal of Toxicology and Environmental Health* 51 (3): 203–218. https://doi.org/10.1080/00984109708984022.

Bustillo Revuelta, M. 2021. "Agglomerated Stone." In *Construction Materials: Geology, Production and Applications*, 91–102. Cham, Switzerland: Springer.

Caesarstone. 2021. "Technical Data Manual." https://www.caesarstoneus.com/wp-content/uploads/2021/10/Ceasarstone_CS_TechnicalDataManual-5.pdf.

Carvalho, E. A. S., N. D. F. Vilela, S. N. Monteiro, C. M. F. Vieira, and L. C. D. Silva. 2018. "Novel Artificial

Ornamental Stone Developed with Quarry Waste in Epoxy Composite." *Materials Research* 21 (suppl 1): e20171104. https://doi.org/10.1590/1980-5373-mr-2017-1104.

Castranova, V., D. Porter, L. Millecchia, J. Y. C. Ma, A. F. Hubbs, and A. Teass. 2002. "Effect of Inhaled Crystalline Silica in a Rat Model: Time Course of Pulmonary Reactions." *Molecular and Cellular Biochemistry* 234-235 (1): 177–184. https://doi.org/10.1023/A:1015967017103.

Driscoll, K. E., D. L. Costa, G. Hatch, R. Henderson, G. Oberdörster, H. Salem, and R. B. Schlesinger. 2000. "Intratracheal Instillation as an Exposure Technique for the Evaluation of Respiratory Tract Toxicity: Uses and Limitations." *Toxicological Sciences* 55 (1): 24–35. https://doi.org/10.1093/toxsci/55.1.24.

Farcas, M. T., W. McKinney, C. Qi, K. W. Mandler, L. Battelli, S. A. FriendA. B. Stefaniak, et al. 2020. "Pulmonary and Systemic Toxicity in Rats Following Inhalation Exposure of 3-D Printer Emissions from Acrylonitrile Butadiene Styrene (ABS) Filament." *Inhalation Toxicology* 32 (11–12): 403–418. https://doi.org/10.1080/08958378.2020.1834034.

Fazio, J. C., S. A. Gandhi, J. Flattery, A. Heinzerling, N. Kamangar, N. Afif, K. J. Cummings, and R. Harrison. 2023. "Silicosis Among Immigrant Engineered Stone (Quartz) Countertop Fabrication Workers in California." *JAMA Internal Medicine* 183 (9): 991–998. https://doi.org/10.1001/jamainternmed.2023.3295.

Fubini, B., and A. Hubbard. 2003. "Reactive Oxygen Species (ROS) and Reactive Nitrogen Species (RNS) Generation by Silica in Inflammation and Fibrosis." *Free Radical Biology and Medicine* 34 (12): 1507–1516. https://doi.org/10.1016/S0891-5849(03)00149-7.

Grand View Research. 2023. Countertops Market Size, Share & Trends Analysis Report by Material (Engineered Quartz, Granite), by End-User (Residential, Commercial), by Application (Bathroom, Kitchen), by Region, and Segment Forecasts, 2023–2030. https://www.grandviewresearch.com/industry-analysis/countertops-market-report.

Hnizdo, E., and V. Vallyathan. 2003. "Chronic Obstructive Pulmonary Disease Due to Occupational Exposure to Silica Dust: A Review of Epidemiological and Pathological Evidence." *Occupational and Environmental Medicine* 60 (4): 237–243. https://doi.org/10.1136/oem.60.4.237.

Hornung, V., F. Bauernfeind, A. Halle, E. O. Samstad, H. Kono, K. L. Rock, K. A. Fitzgerald, and E. Latz. 2008. "Silica Crystals and Aluminum Salts Activate the NALP3 Inflammasome Through Phagosomal Destabilization." *Nature Immunology* 9 (8): 847–856. https://doi.org/10.1038/ni.1631.

Hoy, R. F., C. Dimitriadis, M. Abramson, D. C. Glass, S. Gwini, F. Hore-Lacy, J. Jimenez-Martin, K. Walker-Bone, and M. R. Sim. 2023. "Prevalence and Risk Factors for Silicosis Among a Large Cohort of Stone Benchtop Industry Workers." *Occupational and Environmental Medicine* 80 (8): 439. https://doi.org/10.1136/oemed-2023-108892.

Kacew, S., and E. Demir. 2025. "Absence of Adverse Effects on Pulmonary Histopathology and Functions Following Inhalation Exposure to Chloromethylisothiaolinone/Methylisothiaolinone." *Toxics* 13 (6): 482. https://doi.org/10.3390/toxics13060482.

Komai, M., K. Mihira, A. Shimada, I. Miyamoto, K. Ogihara, Y. Naya, T. Morita, K. Inoue, and H. Takano. 2019. "Pathological Study on Epithelial-Mesenchymal Transition in Silicotic Lung Lesions in Rat." *Veterinary Sciences* 6 (3): 75. https://doi.org/10.3390/vetsci6030070.

Kramer, M. R., P. D. Blanc, E. Fireman, A. Amital, A. Guber, N. A. Rhahman, and D. Shitrit. 2012. "Artificial Stone Silicosis: Disease Resurgence Among Artificial Stone Workers." *Chest* 142 (2): 419–424. https://doi.org/10.1378/chest.11-1321.

Li, M., F. Luan, Y. Zhao, H. Hao, Y. Zhou, W. Han, and X. Fu. 2016. "Epithelial-Mesenchymal Transition: An Emerging Target in Tissue Fibrosis." *Experimental Biology and Medicine (Maywood)* 241 (1): 1–13. https://doi.org/10.1177/1535370215597194.

Lofgren, D. J. 2008. "Results of Inspections in Health Hazard Industries in a Region of the State of Washington." *Journal of Occupational and Environmental Hygiene* 5 (6): 367–379. https://doi.org/10.1080/15459620802066133.

Millerick-May, M. L., S. Schrauben, M. J. Reilly, and K. D. Rosenman. 2015. "Silicosis and Chronic Renal Disease." *American Journal of Industrial Medicine* 58 (7): 730–736. https://doi.org/10.1002/ajim.22465.

OSHA (Occupational Safety and Health Administration). 2015. *Worker Exposure to Silica During Countertop Manufacturing, Finishing and Installation*. Washington, DC: U.S. Department of Labor.

Pascual, S., I. Urrutia, A. Ballaz, I. Arrizubieta, L. Altube, and C. Salinas. 2010. "Prevalence of Silicosis in a Marble Factory After Exposure to Quartz Conglomerates." *Archivos de Bronconeumologia* 47 (1): 50–51. https://doi.org/10.1016/S1579-2129(11)70008-8.

Pavan, C., M. Polimeni, M. Tomatis, I. Corazzari, F. Turci, D. Ghigo, G. G. Grosa, and B. Fubini. 2016. "Editor's Highlight: Abrasion of Artificial Stones as a New Cause of an Ancient Disease. Physicochemical Features and Cellular Responses." *Toxicological Sciences* 153 (1): 4–17. https://doi.org/10.1093/toxsci/kfw101.

Perez-Alonso, A., J. A. Cordoba-Dona, J. L. Millares-Lorenzo, E. Figueroa-Murillo, C. Garcia-Vadillo, and J. Romero-Morillos. 2014. "Outbreak of Silicosis in Spanish Quartz Conglomerate Workers." *International Journal of Occupational and Environmental Health* 20 (1): 26–32. https://doi.org/10.1179/2049396713Y.0000000049.

Phillips, M. L., D. L. Johnson, and A. C. Johnson. 2013. "Determinants of Respirable Silica Exposure in Stone Countertop Fabrication: A Preliminary Study." *Journal of Occupational and Environmental Hygiene* 10 (7): 368–373. https://doi.org/10.1080/15459624.2013.789706.

Pollard, K. M. 2016. "Silica, Silicosis, and Autoimmunity." *Frontiers in Immunology* 7:97. https://doi.org/10.3389/fimmu.2016.00097.

Porter, D. W., A. F. Hubbs, R. R. Mercer, V. A. Robinson, D. M. Ramsey, J. L. McLaurinA. Khan, et al. 2004.

"Progression of Lung Inflammation and Damage in Rats After Cessation of Silica Inhalation." *Toxicological Sciences* 79 (2): 370–380. https://doi.org/10.1093/toxsci/kfh110.

Porter, D. W., L. Millecchia, V. A. Robinson, A. Hubbs, P. Willard, D. PackD. Ramsey, et al. 2002. "Enhanced Nitric Oxide and Reactive Oxygen Species Production and Damage After Inhalation of Silica." *American Journal of Physiology-Lung Cellular and Molecular Physiology* 283 (2): L485–L493. https://doi.org/10.1152/ajplung.00427.2001.

Qi, C., and A. Echt. 2016. "Engineering Control of Silica Dust from Stone Countertop Fabrication and Installation: In-Depth Field Survey Report for the Houston, TX Field Survey." In *EPHB Report No. 375-11a*, Cincinnati, OH: National Institute for Occupational Safety and Health.

Qi, C., and L.-M. Lo. 2016. "Engineering Control of Silica Dust from Stone Countertop Fabrication and Installation: In-Depth Field Survey Report for the Mendota Heights, MN Field Survey." In *EPHB Report No. 375-12a*, Cincinnati, OH: National Institute for Occupational Safety and Health.

Ramkissoon, C., S. Gaskin, T. Hall, D. Pisaniello, and G. Zosky. 2022. "Engineered Stone Fabrication Work Releases Volatile Organic Compounds Classified as Lung Irritants." *Annals of Work Exposures and Health* 67 (2): 288–293. https://doi.org/10.1093/annweh/wxac068.

Ramkissoon, C., S. Gaskin, L. Thredgold, T. Hall, S. Rowett, and R. Gun. 2022. "Characterisation of Dust Emissions from Machined Engineered Stones to Understand the Hazard for Accelerated Silicosis." *Scientific Reports* 12 (1): 4351. https://doi.org/10.1038/s41598-022-08378-8.

Ramkissoon, C., Y. Song, S. Yen, K. Southam, S. Page, D. Pisaniello, S. Gaskin, and G. R. Zosky. 2024. "Understanding the Pathogenesis of Engineered Stone-Associated Silicosis: The Effect of Particle Chemistry on the Lung Cell Response." *Respirology* 29 (3): 217–227. https://doi.org/10.1111/resp.14625.

Ronsmans, S., L. Decoster, S. Keirsbilck, E. Verbeken, and B. Nemery. 2018. "Artificial Stone-Associated Silicosis in Belgium." *Occupational and Environmental Medicine* 76 (2): oemed–2018. https://doi.org/10.1136/oemed-2018-105436.

Rose, C., A. Heinzerling, K. Patel, C. Sack, J. Wolff, L. Zell-BaranD. Weissman, et al. 2019. "Severe Silicosis in Engineered Stone Fabrication Workers — California, Colorado, Texas, and Washington, 2017–2019." *Morbidity & Mortality Weekly Report* 68 (38): 813–818. https://doi.org/10.15585/mmwr.mm6838a1.

Santos, G. G., M. C. Crovace, and E. D. Zanotto. 2019. "New Engineered Stones: Development and Characterization of Mineral-Glass Composites." *Composites Part B Engineering* 167:556–565. https://doi.org/10.1016/j.compositesb.2019.03.010.

Sato, T., T. Shimosato, and D. M. Klinman. 2018. "Silicosis and Lung Cancer: Current Perspectives." *Lung Cancer (Auckland)* 9:91–101. https://doi.org/10.2147/LCTT.S156376.

She, Y. X., Q. Y. Yu, and X. X. Tang. 2021. "Role of Interleukins in the Pathogenesis of Pulmonary Fibrosis." *Cell Death Discovery* 7 (1): 52. https://doi.org/10.1038/s41420-021-00437-9.

Stone, R. C., I. Pastar, N. Ojeh, V. Chen, S. Liu, K. I. Garzon, and M. Tomic-Canic. 2016. "Epithelial-Mesenchymal Transition in Tissue Repair and Fibrosis." *Cell and Tissue Research* 365 (3): 495–506. https://doi.org/10.1007/s00441-016-2464-0.

Thibodeau, M. S., C. Giardina, D. A. Knecht, J. Helble, and A. K. Hubbard. 2004. "Silica-Induced Apoptosis in Mouse Alveolar Macrophages Is Initiated by Lysosomal Enzyme Activity." *Toxicological Sciences* 80 (1): 34–48. https://doi.org/10.1093/toxsci/kfh121.

Thompson, D., and C. Qi. 2022. "Characterization of the Emissions and Crystalline Silica Content of Airborne Dust Generated from Grinding Natural and Engineered Stones." *Annals of Work Exposures and Health* 67 (2): 266–280. https://doi.org/10.1093/annweh/wxac070.

Umbright, C., R. Sellamuthu, J. R. Roberts, S. H. Young, D. Richardson, D. Schwegler-BerryW. McKinney, et al. 2017. "Pulmonary Toxicity and Global Gene Expression Changes in Response to Sub-Chronic Inhalation Exposure to Crystalline Silica in Rats." *Journal of Toxicology & Environmental Health A* 80 (23–24): 1349–1368. https://doi.org/10.1080/15287394.2017.1384773.

Vallyathan, V., V. Castranova, D. Pack, S. Leonard, J. Shumaker, A. F. Hubbs, D. A. Shoemaker, D. M. Ramsey, J. R. Pretty, and J. L. McLaurin. 1995. "Freshly Fractured Quartz Inhalation Leads to Enhanced Lung Injury and Inflammation: Potential Role of Free Radicals." *American Journal of Respiratory and Critical Care Medicine* 152 (3): 1003–1009. https://doi.org/10.1164/ajrccm.152.3.7663775.

Vallyathan, V., X. Shi, N. S. Dalal, W. Irr, and V. Castranova. 1988. "Generation of Free Radicals from Freshly Fractured Silica Dust. Potential Role in Acute Silica-Induced Lung Injury." *The American Review of Respiratory Disease* 138 (5): 1213–1219. https://doi.org/10.1164/ajrccm/138.5.1213.

van de Veerdonk, F. L., M. G. Netea, C. A. Dinarello, and L. A. B. Joosten. 2011. "Inflammasome Activation and IL-1β and IL-18 Processing During Infection." *Trends in Immunology* 32 (3): 110–116. https://doi.org/10.1016/j.it.2011.01.003.

Wu, R., J. Högberg, M. Adner, P. Ramos-Ramírez, U. Stenius, and H. Zheng. 2020. "Crystalline Silica Particles Cause Rapid NLRP3-Dependent Mitochondrial Depolarization and DNA Damage in Airway Epithelial Cells." *Particle and Fibre Toxicology* 17 (1): 39. https://doi.org/10.1186/s12989-020-00370-2.

Zwack, L. M. V. K., S. E. Brueck, and C. Qi. 2016. *Evaluation of Crystalline Silica Exposure During Fabrication of Natural and Engineered Stone Countertops*. HHE Report No. 2014-0215-3250. Cincinnati, OH: National Institute for Occupational Safety and Health.